

Light dark matter searches with positrons

M. Battaglieri^{1,2}, A. Bianconi^{3,4}, P. Bisio⁵, M. Bondi¹, A. Celentano¹,
G. Costantini^{3,4}, P.L. Cole⁶, L. Darmé⁷, R. De Vita¹, A. D’Angelo^{8,9},
M. De Napoli¹⁰, L. El Fassi¹¹, V. Kozhuharov^{7,12}, A. Italiano¹⁰,
G. Krnjaic^{13,14}, L. Lanza⁸, M. Leali^{3,4}, L. Marsicano^{1,a}, V. Mascagna^{4,15},
S. Migliorati^{3,4}, E. Nardi⁷, M. Raggi^{16,17,a}, N. Randazzo¹⁰, E. Santopinto¹,
E. Smith², M. Spreafico⁵, S. Stepanyan², M. Ungaro², P. Valente¹⁷,
L. Venturelli^{3,4}, M.H. Wood¹⁸

¹Istituto Nazionale di Fisica Nucleare, Sezione di Genova, 16146 Genova, Italy

²Thomas Jefferson National Accelerator Facility, Newport News, Virginia 23606

³Università degli Studi di Brescia, 25123 Brescia, Italy

⁴INFN, Sezione di Pavia, 27100 Pavia, Italy

⁵Università degli Studi di Genova, 16146 Genova, Italy

⁶Lamar University, 4400 MLK Blvd, PO Box 10046, Beaumont, Texas 77710

⁷Istituto Nazionale di Fisica Nucleare, Laboratori Nazionali di Frascati, Via E. Fermi 54, Frascati, Italy

⁸INFN, Sezione di Roma Tor Vergata, 00133 Rome, Italy

⁹Università di Roma Tor Vergata, 00133 Rome Italy

¹⁰Istituto Nazionale di Fisica Nucleare, Sezione di Catania, 95125 Catania, Italy

¹¹Mississippi State University, Mississippi State, Mississippi 39762-5167, USA

¹²Faculty of physics, University of Sofia, 5 J. Bourchier Blvd., 1164 Sofia, Bulgaria

¹³Fermi National Accelerator Laboratory, Batavia, Illinois 60510, USA

¹⁴Kavli Institute for Cosmological Physics, University of Chicago, Chicago, Illinois 60637, USA

¹⁵Università degli Studi dell’Insubria, 22100 Como, Italy

¹⁶Sapienza Università di Roma, piazzale Aldo Moro 5 Roma, Italy

¹⁷Istituto Nazionale di Fisica Nucleare, Sezione di Roma, piazzale Aldo Moro 5 Roma, Italy

¹⁸Canisius College, Buffalo, NY 14208, USA

Draft : February 8, 2022

Abstract We discuss two complementary strategies to search for light dark matter (LDM) exploiting the positron beam possibly available in the future at Jefferson Laboratory. LDM is a new compelling hypothesis that identifies dark matter with new sub-GeV “hidden sector” states, neutral under standard model interactions and interacting with our world through a new force. Accelerator-based searches at the intensity frontier are uniquely suited to explore it. Thanks to the high intensity and the high energy of the CEBAF (Continuous Electron Beam Accelerator Facility) beam, and relying on a novel LDM production mechanism via positron annihilation on target atomic electrons, the proposed strategies will allow us to explore new regions in the LDM parameters space, thoroughly probing the LDM hypothesis as well as more general hidden sector scenarios.

1 Introduction and motivations

One of the most compelling arguments motivating the search for extensions of the Standard Model (SM) is the need to explain the nature of dark matter (DM). In years past, theoretical and experimental efforts mainly catalysed around the hypothesis that DM corresponds to a Weakly Interacting Massive Particle (WIMP) with electroweak scale mass. Such a hypothesis is well grounded since in the early Universe WIMPs would be produced via thermal processes, and their annihilation with typical weak interaction rates would leave, almost independently of other details, a relic density of the correct size to explain DM observations. However, despite an extensive search program that combined direct, indirect, and collider probes, to date no conclusive signal of the WIMP has been found [1]. This prompts the scientific community to put no lesser vigor in exploring alternative pathways.

Feebly interacting particles (FIPs) represent a particularly interesting alternative to WIMPs. In recent years the physics of FIPs has focused a steadily growing

^aContact authors: luca.marsicano@ge.infn.it,
mauro.raggi@roma1.infn.it

interest, as characterised witnessed by the remarkable number of community reports and white papers that have appeared in the last few years [2, 3, 4, 5, 6, 7]. FIPs are exotic and relatively light particles, not charged under the SM gauge group, whose interactions with the SM fields are extremely suppressed. FIPs are often assumed to be part of a possibly complicated secluded sector, called the *dark sector*, with the Lightest stable dark particle(s) playing the role of DM (LDM). This scenario has sound theoretical motivations: in first place many known particles are uncharged under some gauge group factors, so that the existence of particles blind to all $SU(3)_C \times SU(2)_L \times U(1)_Y$ interactions seems a rather natural possibility. Secondly, theoretical mechanisms like gauge symmetries or quasi-exact spontaneously broken global symmetries, that we know are realised in Nature, can explain why some particles remain light even when they are associated with physics at some large scale. From the phenomenological point of view, light weakly coupled new particles have been often invoked to account for several discrepancies observed in low energy experiments. Examples are the measured value of the muon anomalous magnetic moment [8], the proton charge radius measured in muonic atoms [9, 10, 11], the discrepancy between neutron lifetime measurements in bottle and beam experiments [12, 13], the measured abundance of primordial ${}^7\text{Li}$ which is a factor of three lower than BBN predictions [14], the ‘bump’ in the angular distribution of e^\pm pairs observed by the Atomki collaboration in nuclear decays of ${}^8\text{Be}$ [15] and ${}^4\text{He}$ [16] excited states.

FIPs scenarios hint to a remarkably broad range of possibilities, ranging from the very nature of the new particles (scalars, pseudoscalars, fermions, spin-one bosons) and spanning several order of magnitude in mass and couplings. To thoroughly explore all these possibilities will require an extensive collaboration among a variety of small/medium scale experiments, exploiting diversified detection techniques, and operating at different facilities. Accelerator-based searches exploiting positron beams stand out as a particularly powerful tool. This is because for any given beam energy there is a range of masses where dark bosons can be produced resonantly through positron annihilation on atomic electrons in the target, yielding a huge enhancement in the production rate. As it was first pointed out in Ref. [17], for resonant production there is no need that the beam energy will be tuned to match in the c.m. the precise value of the mediator mass. This is because due to the continue loss of energy from soft photon bremsstrahlung, in the first few radiation lengths of a dump a positron beam can continuously scan for production of new resonances. While it was later recog-

nised that this process is of more general importance since, due to the presence of secondary positrons in EM showers, it contributes to FIPs production also in electron [18, 19] and proton [20] beam experiments, it is clear that the availability of a beam of primary positrons is of utmost importance to fully take advantage of the resonant production channel.

1.1 Dark sectors and relic density targets

Experimental proposals aiming at detecting missing energy from the apparatus are mostly sensitive to the FIPs nature and couplings. While this allows such search strategies to cover a broad class of new light physics models, the details of the dark sector to which the DM belongs remain ultimately inaccessible. Relic density targets thus must rely on additional theoretical assumptions. Arguably the most elegant models for LDM are those which reproduce the successes of WIMP models, being: UV-insensitive, predictive and as economical as possible. A generic expectation is then that DM annihilation proceeds via a bosonic feebly-interacting mediator, taking care that by the time of CMB annihilation is sufficiently suppressed to evade standard limits on energy injection [21, 22, 23].

Various simplified structures for the dark sector itself have been considered throughout the years, ranging from basic scenarios such as a complex scalar DM to more advanced setups as asymmetric DM or inelastic DM with an additional dark Higgs boson. The broad target region where $\Omega_{\text{DM}} h^2 = 0.11933 \pm 0.00091$ [23] corresponds to mediator FIPs in the 1 MeV – 10 GeV mass window with coupling suppressed as $10^{-5} - 10^{-2}$ respectively. However, the precise relic density target strongly depends on the details of the model. Assuming for simplicity a dark photon A' scenario, interaction with the SM can proceed via a kinetic mixing ε . The dark photon couples with the electromagnetic current $\mathcal{J}_{\text{em}}^\mu$ with coupling $e\varepsilon$ and with the dark gauge current $\mathcal{J}_{\text{D}}^\mu$ leading to:

$$\mathcal{L} \supset -A'_\mu e\varepsilon \mathcal{J}_{\text{em}}^\mu - A'_\mu g_D \mathcal{J}_{\text{D}}^\mu. \quad (1)$$

Different DM candidates corresponds to different choices of dark currents (see e.g. a summary in [24]) and different thermal targets:

$$\mathcal{J}_{\text{D}}^\mu = \begin{cases} i(\chi^* \partial^\mu \chi - \chi \partial^\mu \chi^*) & (\text{Complex Scalar DM, } \chi) \\ \frac{1}{2} \bar{\chi} \gamma^\mu \gamma^5 \chi & (\text{Majorana DM, } \chi) \\ i \bar{\chi}_1 \gamma^\mu \chi_2 & (\text{pseudo-Dirac DM, } \chi_1) \end{cases}$$

In the simplest cases where the DM relic density is fixed completely via the freeze-out of a dark photon-induced

s -channel annihilation, the final relic density depends only on one variable that, for $m_\chi \ll m_{A'}$, reads:

$$y \equiv \varepsilon^2 \alpha_D \left(\frac{m_\chi}{m_{A'}} \right)^4. \quad (2)$$

Depending on the DM nature the typical values of y required to match the relic density target can vary by a few orders of magnitude. A simple example of the effect of the dark sector structure on the relic density is found in the inelastic DM scenario (see [25, 26] and subsequent literature). The dominant annihilation channel at low masses, $\chi_1 \chi_2 \rightarrow A'^* \rightarrow e^+ e^-$, depends on the mass splitting between the states (co-annihilation mechanism [27, 28]) as well as on whether the mediator can be produced resonantly when $m_{\chi_1} + m_{\chi_2} \lesssim m_{A'}$ (resonant annihilation mechanism [27, 29]). The former suppresses exponentially the annihilation rate, thus greatly increasing the thermal target in y , while the latter enhances the annihilation, decreasing the thermal target. Finally, the presence of a dark Higgs boson, typically required in UV realisation of this scenario can open additional annihilation channels [30, 31, 32].

Although LDM models represent a particularly interesting target, the experimental setups described in this work can be used more generally to search for a large range of FIPs. In particular the limits shown in the case of a dark photon straightforwardly apply to any invisibly-decaying vector boson with coupling to electron/positron g_e with the matching $g_e \leftrightarrow e\varepsilon$. In the case of a (pseudo)-scalar mediator (resp. axion-like particle) with coupling y_e (resp. $g_{ae}m_e$) we have, away from the kinematic threshold, the approximate equivalence $e\bar{e} \leftrightarrow y_e/\sqrt{2} \leftrightarrow g_{ae}m_e/\sqrt{2}$ where the $\sqrt{2}$ arises from the different number of degrees of freedom.

2 Dark sector searches with positron beams on fixed targets

The production of LDM particles can be generated in collisions of electrons or positrons of several GeV with a fixed target by the processes depicted in Fig. 1, with the final state A' decaying to a $\chi\bar{\chi}$ pair. For experiments with electron beams, diagram (a), analogous to ordinary photon bremsstrahlung, is the dominant process, although it was recently shown that for thick-target setups, where positrons are generated as secondaries from the developing electromagnetic shower, diagrams (b) and (c) give non-negligible contributions for selected regions of the parameters space [19] – see Ref. [5] for a comprehensive review of past/current experiments and future proposals. On the other hand, for experiments with positron beams, diagrams (b) and (c) play

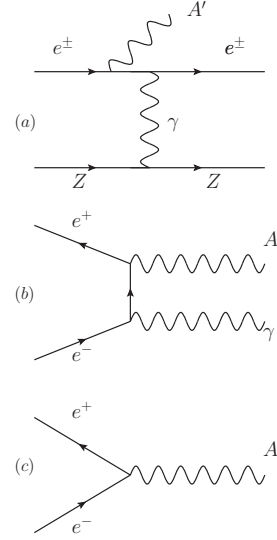


Fig. 1 Three different A' production modes in fixed target lepton beam experiments: (a) A' -strahlung in e^-/e^+ -nucleon scattering; (b) A' -strahlung in e^+e^- annihilation; (c) resonant A' production in e^+e^- annihilation.

the most important role. In this document, we present two complementary measurements to search for light dark matter with positron beams at Jefferson Laboratory, exploiting the unique potential of the proposed e^+ -beam facility. In the following, we introduce the two approaches and, for each one, we briefly discuss the experimental setup, the measurement strategy, the data analysis and the envisioned results. We underline that Jefferson Laboratory is playing a leading role in the LDM searches, with different experiments already running, HPS [33] and APEX [34], or approved to run in the near future, BDX [35] and DarkLight [36].

2.1 Thin-target measurement

This measurement exploits the A' -strahlung production in electron-positron annihilation described by diagram (b). The primary positron beam impinges on a thin target, where a photon- A' is produced. By detecting the final-state photon in an electromagnetic calorimeter, the missing mass kinematic variable M_{miss} can be computed event-by-event:

$$M_{miss}^2 = (P_{beam} + P_{target} - P_\gamma)^2. \quad (3)$$

The signal would show up as a peak in the missing mass distribution, centered at the A' mass, on top of a smooth background due to SM processes resulting from events with a single photon measured in the calorimeter. The peak width is mainly determined by the energy and angular resolution of the calorimeter. Several experiments searching for A' with this approach

have been proposed. PADME (Positron Annihilation into Dark Matter Experiment) at LNF [37] is one of the first e^+ on thin target experiment searching for A' . It uses the 550 MeV positron beam provided by the *DAΦNE* linac at INFN LNF (Laboratori Nazionali di Frascati) impinging on a thin diamond target.

2.2 Active thick-target measurement

This measurement exploits the *resonant A' production* by positrons annihilation on atomic electrons described by diagram (c). The primary positron beam impinges on a thick active target, and the *missing energy* signature of produced and undetected χ is used to identify the signal [38]. The active target measures the energy deposited by the individual beam particles: when an energetic A' is produced, its *invisible* decay products – the $\chi\bar{\chi}$ pair – will carry away a significant fraction of the primary beam energy, thus resulting in measurable reduction in the expected deposited energy. Signal events are identified when the *missing energy* E_{miss} , defined as the difference between the beam energy and the detected energy, exceeds a minimum threshold value. The signal has a very distinct dependence on the missing energy through the relation¹ $m_{A'} = \sqrt{2m_e E_{miss}}$. This results in a specific experimental signature for the signal, that would appear as a peak in the missing energy distribution, at a value depending solely on the dark photon mass. Thanks to the emission of soft bremsstrahlung photons, the thick target provides an almost continuous energy loss for the impinging positrons. Even though the positron energy loss is a quantized process, the finite intrinsic width of the dark photon – much larger than the positron energies differences – and the electrons energy and momentum spread induced by atomic motions [17] will indeed compensate this effect. This allows the primary beam to “scan” the full range of dark photon masses from the maximum value (corresponding to the loss of all the beam energy), to the minimum value fixed by the missing energy threshold [18], exploiting the presence of secondary positrons produced by the developing electromagnetic shower.

3 Positron annihilation on a thin target

3.1 Signal signature and yield

The differential cross section for dark photon production via the positron annihilation on the atomic electron

¹ $m_{A'}$ is the dark photon mass and $m_e = 0.511$ MeV/ c^2 is the electron mass.

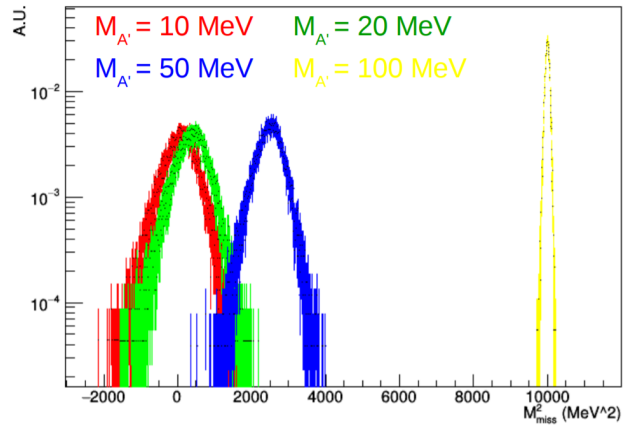


Fig. 2 Computed missing mass spectrum for signal events for 4 different values of $m_{A'}$.

of the target $e^+e^- \rightarrow A'\gamma$, is given by:

$$\frac{d\sigma}{dz} = \frac{4\pi\alpha^2\varepsilon^2}{s} \left(\frac{s - m_{A'}^2}{2s} \frac{1 + z^2}{1 - \beta^2 z^2} + \frac{m_{A'}^2}{s - m_{A'}^2} \frac{1}{1 - \beta^2 z^2} \right).$$

Here s is the e^+e^- system invariant mass squared, z is the cosine of the A' emission angle in the CM frame, measured with respect to the positron beam axis, and $\beta = \sqrt{1 - \frac{4m_e^2}{s}}$. This result has been derived at tree level, keeping the leading m_e dependence to avoid non-physical divergences when $|z| \rightarrow 1$. The emission of the annihilation products in the CM frame is concentrated in the e^+e^- direction. This results in an angular distribution for the emitted γ peaked in the forward direction in the laboratory frame. In the case of invisible decays, the A' escapes detection, while the γ can be detected in the downstream electromagnetic calorimeter (ECAL). The measurement of the photon energy and emission angle, together with the precise knowledge of the primary positron momentum, allows computing the missing mass kinematic variable from Eq. 3. The mass range that can be spanned is constrained by the available energy in the center of mass frame: using an 11 GeV positron beam at JLab, A' masses up to ~ 106 MeV/ c^2 can be explored. The signal yield has been evaluated using CALCHEP [39]; the widths $\sigma(m_{A'})$ of the missing mass distributions of the measured recoil photon has been computed for six different values of the A' mass value in the 1–103 MeV range. CALCHEP provides the total cross section of the process, for $\varepsilon = 1$; the cross section value as a function of ε has been obtained multiplying it by ε^2 . Figure 2 shows results for 4 mass values: due to the $e^+e^- \rightarrow \gamma A'$ process kinematics, the missing mass resolution for the signal is best for large A' masses and degraded for a “light” A' ($m_{A'} < 50$ MeV).

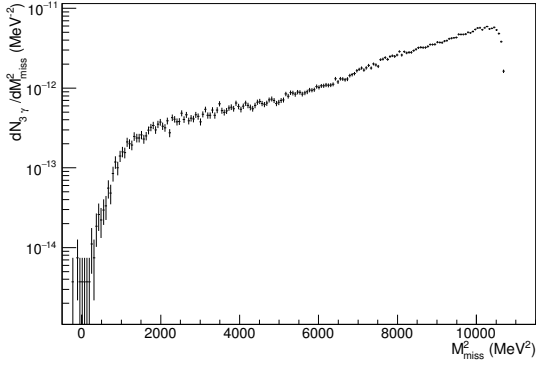


Fig. 3 Differential missing mass spectrum from positron annihilation into three photons events, normalized to single positron on target.

3.2 Expected background

All processes resulting in a single γ hitting the calorimeter represent the background for the experiment, the most relevant being *bremsstrahlung* and the e^+e^- annihilation processes in two and three photons. In order to reduce the *bremsstrahlung* background, the proposed detector features an active veto system composed of plastic scintillating bars: positrons losing energy via *bremsstrahlung* in the target are detected in the vetoes, rejecting the event. However the high *bremsstrahlung* rate is an issue for this class of experiments, limiting the maximum viable beam current. To evaluate this background, a full GEANT4 [40] simulation of the positron beam impinging on the target, based on the PadmeMC simulation program [41], has been performed. For all *bremsstrahlung* photons reaching the ECAL, the missing mass has been computed, accounting for the assumed detector angular and momentum resolution.

The $e^+e^- \rightarrow \gamma\gamma$ and $e^+e^- \rightarrow \gamma\gamma\gamma$ annihilation processes can produce background events whenever only one of the produced photons is detected in the ECAL. This contribution to background has been calculated as follows. Events have been generated directly using CALCHEP, which provided also the total cross sections for the processes. As in the case of *bremsstrahlung*, the missing mass spectrum was computed for events with a single photon hit in the ECAL. This study proved that, if one requires the measured energy to be greater than 600 MeV, the two photon annihilation background becomes negligible. This is due to momentum conservation: asking for only one photon to fall within the ECAL geometrical acceptance translates in a strong constraint on its energy. This argument does not apply to the three-photon annihilation: this process generates an irreducible background for the experiment (see Fig. 3

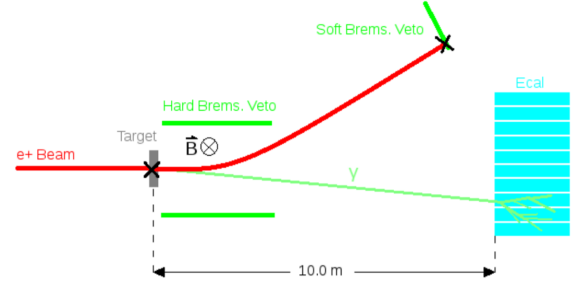


Fig. 4 Layout of the proposed thin target setup.

for the missing mass spectrum produced by the three-photon annihilation).

3.3 Experimental Setup

The experimental setup of the proposed measurement is shown in Fig. 4. The 11 GeV positron beam impinges on a 100- μm thick target made of carbon, which is a good compromise between density and a low Z/A ratio allowing to reduce the *bremsstrahlung* rate. A magnet capable of generating a field of 1 T over a region of 2 m downstream the target bends the charged particles (including non-interacting positrons) away from the ECAL, placed a few meters downstream. The ECAL is composed of high density scintillating crystals, arranged in a cylindrical shape. High segmentation is necessary to obtain a good angular resolution, critical for a precise missing mass computation, but should however be matched with the Molière radius of the chosen material.

Crystals of PbWO_4 , $\text{LSO}(\text{Ce})$ and BGO , represent optimal choices, given the fast scintillating time, high-density and short radiation length. Energy resolution, as well as angular resolution, play a crucial role in the missing mass computation; a value of $\frac{\sigma(E)}{E} = \frac{2\%}{\sqrt{E}}$ has been assumed for this study, consistent with the performance of the 23-cm long PADME BGO detector, corresponding to 20 radiation lengths. Such a depth is indeed needed for achieving this performance, due to longitudinal shower containment. Since the small-angle *bremsstrahlung* high rate would blind the central crystals of the calorimeter, the simplest solution is to imagine a hole at the center of the cylinder. An indicative value of 50 cm for the calorimeter radius and a distance from the target of 10 m were assumed in the evaluation of the projected sensitivity of this experiment. With a spatial resolution of ~ 5 mm for the photon impact position, an angular resolution of 0.5 mrad and a geometrical acceptance of ~ 50 mrad are achieved.

With a view to adapting the existing PADME detector to perform this measurement – as thoroughly

discussed below – the assumed acceptance and resolution can be achieved with the 30 cm radius PADME calorimeter, placed at a 6 m distance from the target. In PADME, with a crystal front-face of $20 \times 20 \text{ mm}^2$, a spatial resolution of $\sim 3.5 \text{ mm}$ has been measured (significantly better than $20 \text{ mm} / \sqrt{12}$). At 6 m distance this corresponds to an angular resolution of 0.5 mrad and an acceptance of $\sim 50 \text{ mrad}$, consistent with the assumed parameters.

Besides the ECAL, the experimental setup includes a veto system to reduce the bremsstrahlung background. Following the layout of the PADME experiment, the vetoes are composed of plastic scintillator bars. Whenever the primary e^+ loses energy via bremsstrahlung in the target, its trajectory is bent by the magnetic field and it impinges on the veto bars, rejecting the event. For the sake of this study, a 99.5% veto efficiency has been considered. This assumption is proven realistic by the performance of the existing PADME experiment veto system [37]. Although this option was not considered in this study, further suppression of the background can be achieved by placing a photon detector, much faster than the main calorimeter, covering its central hole. Such a fast calorimeter would also help in the reduction of $\gamma\gamma$ and 3γ events with one or two photons lost. In the case of PADME a 5×5 matrix of $3 \times 3 \text{ cm}^2$ PbF_2 crystals is used. The Cherenkov light from showers is readout by fast photomultipliers, providing a $\sim 2 \text{ ns}$ double pulse separation (to be compared with $\sim 300 \text{ ns}$ decay time of the BGO).

3.4 Positron beam requirements

As already mentioned, the A' mass range that the proposed thin target experiment can explore is strictly constrained by the available energy in the center of mass frame. In this respect, a 11 GeV positron beam would allow extending significantly the A' mass range with respect to other similar experiments, up to $\sim 106 \text{ MeV}/c^2$. Being the $e^+e^- \rightarrow \gamma A'$ annihilation a rare process, the sensitivity of the proposed search depends on the number of positron on target (POT) collected. In this setup, the maximum current is constrained by the bremsstrahlung rate on the ECAL innermost crystals. Therefore, a continuous beam structure is preferable. In this study, a continuous 100-nA beam has been considered, resulting in a manageable $\sim 200\text{-kHz}$ rate per crystal in the inner ECAL. In this configuration, 10^{19} POT can be collected in 180 days, covering a new region in the A' parameter space. In the event that the available beam current is lower than 100 nA, a similar result can be obtained increasing the target thickness, at the price of a higher background due to multiple scattering.

The computation of the missing mass requires a precise knowledge of the primary positron momentum; this translates to certain requirements in terms of the quality of the beam. Here, a energy dispersion $\frac{\sigma_{E_{Beam}}}{E_{Beam}} < 1\%$ and an angular dispersion $\theta_{Beam} < 0.1 \text{ mrad}$ of the beam have been considered. With these assumptions, the missing mass resolution is dominated by the ECAL performance, with a negligible contribution from the beam dispersion.

3.5 Reuse of the PADME components

It's also interesting to investigate the possibility of reusing the existing PADME experimental apparatus as the starting point for the new thin target experiment at the CEBAF accelerator. In this paper we try to shortly review which part of the apparatus could be directly reused, and which will need to be adapted to the different beam conditions.

The PADME target can be easily transferred and installed in the CEBAF accelerator, while the option of a ticker target will simplify the design and it is easily achievable. The PADME electromagnetic calorimeter performance is adequate with the requirements for the thin target experiment: in addition to the excellent energy resolution, $< 2\%\sqrt{E}$ [42], and spatial resolution, $\sim 3.5 \text{ mm}$, single BGO crystals are capable of tolerating rates in excess of 2 MHz. The increased energy of the beam, from 0.5 to 11 GeV, would improve the energy resolution, but will also enhance the contribution of longitudinal shower containment to the resolution with respect to the stochastic term. The overall effect should not degrade the resolution significantly, due to the sufficient total depth of $\sim 20 X_0$.

The small angle calorimeter will also profit by the much higher energy of the impinging photons, but will suffer more the longitudinal leakage, being only $15 X_0$ long. This will not compromise its use as photon veto, while performance as calorimeter, for improving 2γ and 3γ acceptance, needs to be evaluated.

The charged veto system will certainly require a different geometrical assembly, both due to the need of a longer magnet and the different boost, but the technology and front-end electronics can be reused.

The trigger and DAQ system of the PADME experiment [43] was built to operate at a rate of 50 Hz as imposed by the repetition rate of the DAΦNE LINAC. Currently, PADME is operated in trigger-less mode, i.e. digitizing all channels of the detectors every single beam bunch, typically in a $1 \mu\text{s}$ window (1024 samples at 1 Gsample/s). Of course such a system cannot be used with a continuous beam structure, so that a new trigger and DAQ system need to be designed and built.

4 Positron annihilation on a thick active target

4.1 Signal signature and yield

The cross section for LDM production through positron annihilation on atomic electrons, $e^+e^- \rightarrow A' \rightarrow \chi\bar{\chi}$, is characterised by a resonant shape [44]:

$$\sigma = \frac{4\pi\alpha_{EM}\alpha_D\varepsilon^2}{\sqrt{s}} \frac{q(s - 4/3q^2)}{(s - m_{A'}^2)^2 + \Gamma_{A'}^2 m_{A'}^2}, \quad (4)$$

where s is the e^+e^- system invariant mass squared, q is the $\chi - \bar{\chi}$ momentum in the CM frame, and $\Gamma_{A'}$ is the A' width. The kinematics of the $e^+e^- \rightarrow \chi\bar{\chi}$ reaction in the *on-shell scenario* ($m_{A'} > 2m_\chi$) is strongly constrained by the underlying dynamics. Since the A' decays invisibly, its energy is not deposited in the active target, and the corresponding experimental signature is the presence of a peak in the missing energy (E_{miss}) distribution, whose position depends solely on the A' mass through the kinematic relation

$$m_{A'} = \sqrt{2m_e E_{miss}}. \quad (5)$$

For a given A' mass, the expected signal yield is:

$$N_s = n_{POT} \frac{N_A}{A} Z\rho \int_{E_{miss}^{CUT}}^{E_0} dE_e T_+(E_e) \sigma(E_e), \quad (6)$$

where A , Z , ρ , are, respectively, the target material atomic mass, atomic number and mass density, E_0 is the primary beam energy, N_A is Avogadro's number, $\sigma(E_e)$ is the energy-dependent production cross section, n_{POT} is the number of impinging positrons and E_{miss}^{CUT} is the missing energy cut. Finally, $T_+(E_e)$ is the positrons differential track-length distribution [45], reported in Fig. 5 for a 11 GeV positron beam.

4.2 Positron beam requirements

A missing energy measurement requires that the intensity of the primary positron beam is low enough so that individual e^+ impinging on the active target can be distinguished. At the same time, the beam current has to be large enough to accumulate a sizeable number of positrons on target (POT). For example, a positron beam with a time structure corresponding to $1 e^+/\mu s$ can accumulate more than 10^{13} POT/year, with an average time interval between positrons of $1 \mu s$.

This specific time structure is challenging for the proposed CEBAF e^+ operations. In particular, the low beam current, ~ 0.1 pA, is incompatible with the standard beam diagnostic tools that are employed to properly steer and control the CEBAF beam. Therefore, the following “mixed operation mode” is currently being

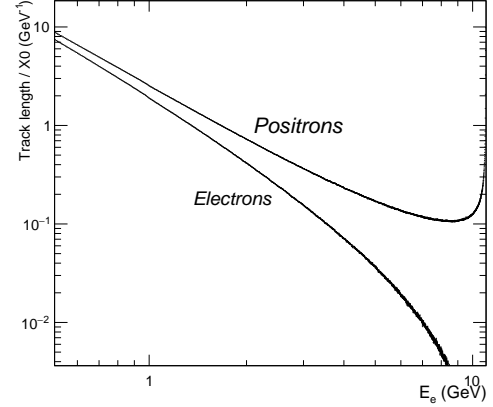


Fig. 5 Differential positrons track length distribution, normalized to the radiation length, for a 11 GeV e^+ beam impinging on a thick target. For comparison, the same distribution in case of an impinging electron beam is reported.

considered for the experiment (see also Fig. 6) [46]. A $10\text{-}\mu s$ long 100 nA *diagnostic macro-pulse* is injected in the CEBAF accelerator with a 60 Hz frequency. This results to an average current of 60 pA, with a peak current large enough to enable proper operation of the beam diagnostic systems. In between every pulse, low intensity *physics pulses*, populated *on average* by less than $1 e^+$, are injected at higher frequency.

This challenging operation scheme can be realized using an ad-hoc laser system at the injector. With dedicated R&D, it would be possible to design and construct a system capable of injecting fast bunches at 31.25 MHz - i.e. one bunch every 32 ns. Since the (discrete) number of positrons per bunch follows a Poissonian statistical distribution, the time interval between e^+ can be further increased by reducing the average bunch population, by adjusting the laser intensity. A ~ 500 ns spacing between positrons can be obtained by using an average laser power of $0.05 e^+/\text{bunch}$. The experiment will acquire data only during low-intensity pulses, ignoring the $10 \mu s$ long high current periods. However, if all these positrons would impact on the detector, the average rate of $\sim 3.7 \cdot 10^8 e^+/\text{s}$ would result in a very large radiation dose deposited in the active target. To avoid this, we plan to install in front of the detector a fast magnetic deflector, synchronized to the beam 60 Hz frequency, in order to transport the positrons belonging to the high-current pulses to a suitable beam-dump, avoiding their impact on the detector.

In summary, the proposed CEBAF operation mode would allow to obtain a beam with positrons impinging on the detector on average every ~ 500 ns, compatible with the accelerator control and diagnostic system. It should be remarked that this technical solution requires

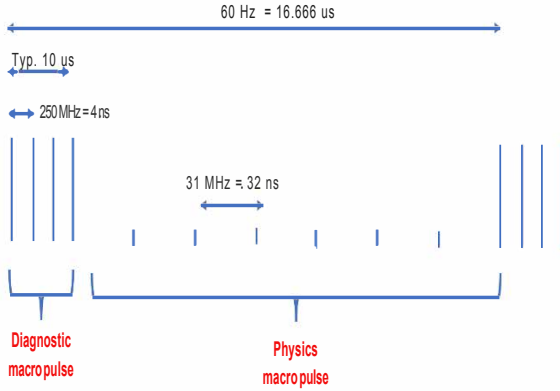


Fig. 6 Simplified scheme of the e^+ beam time structure for the thick-target measurements, see text for details.

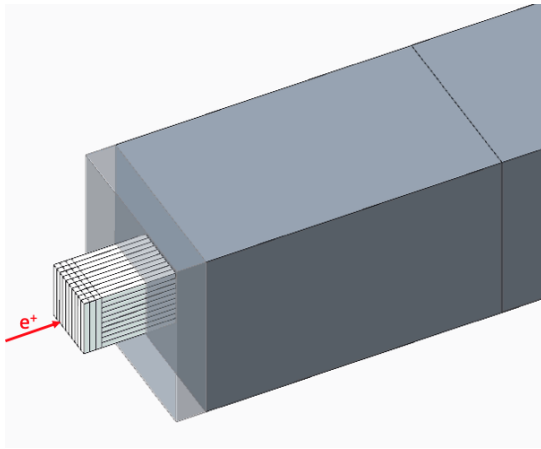


Fig. 7 Schematic layout of the active thick-target experimental setup, with the ECAL (white) followed and surrounded by the HCAL (grey). The semi-transparent portion of the HCAL in front is that installed all around the ECAL.

R&D activities, that are already (partially) planned in the contest of EIC accelerator development. In the following, we will present the sensitivity to DM considering 10^{13} POT accumulated in one year of run.

4.3 Experimental setup

The layout of the proposed measurement is schematically reported in Fig. 7. It includes a homogeneous electromagnetic calorimeter (ECAL) acting as a thick target to measure the energy of each impinging positron, and a hadron detection system (HCAL) installed around and downstream the active target to measure long-lived (neutrons/ K_L) or highly penetration (muons/charged pions) particles escaping from the ECAL.

The *preliminary* ECAL design foresees a 28 radiation lengths detector, made as a 10×10 matrix of PbWO_4 crystals of dimensions of $20 \times 20 \times 250 \text{ mm}^3$. Three layers of crystals are added in front, with the

long axis oriented perpendicular to the beam direction, to act as a preshower, resulting in a total calorimeter length of $35X_0$. The choice of PbWO_4 material is motivated by its fast scintillating time ($\tau \simeq 30 \text{ ns}$), well matched to the expected hit rate, its high-density, resulting in a compact detector, and its high radiation hardness. The total calorimeter length was selected to limit below $\sim 10^{-13}$ per POT the probability that any particle from the developing cascade, in particularly photons, escape the detector faking a signal. The transverse size, was chosen to provide measurements of the shower transverse profile and to optimize the optical matching with the light sensor. The total front face size ($20 \times 20 \text{ cm}^2$) is large enough to avoid transverse energy leakage affecting the detector resolution. SiPMs will be used to collect scintillation light from the crystals. The use of these sensors has never been adopted so far in high-energy electromagnetic calorimetry with PbWO_4 crystals, and requires a careful selection of the corresponding parameters. First measurements on PbWO_4 crystals with $6 \times 6 \text{ mm}^2$ devices having a $25 \mu\text{m}$ pixel size show a light yield of $\sim 1 \text{ phe} / \text{MeV}$, compatible with the experiment requirements (energy resolution and dynamic range). The expected radiation dose for the detector, for positrons impinging on the calorimeter every 500 ns and assuming an overall beam availability of 50% is, at maximum, $\sim 350 \text{ rad/h}$, corresponding to the central crystals. This large value, comparable to the maximum dose in the CMS PbWO_4 electromagnetic calorimeter [47, 48], calls for a careful calorimeter design and for the identification of procedures to mitigate any possible radiation damage during detector operation. These include varying the beam impact point on the detector to distribute the radiation dose across crystals, as well as annealing crystals during off-beam operations, exploiting both thermal annealing and light-induced processes [49, 50].

The main requirement for the HCAL is the hermeticity to long-lived particles exiting from the ECAL. From a Montecarlo simulation of this setup, the probability of having one or more high-energy ($\gtrsim 1 \text{ GeV}$) hadron leaving the active target is $\sim 10^{-4}$ per POT. This calls for a HCAL inefficiency of 10^{-10} or lower. The *preliminary* detector design uses a modular iron/scintillator inhomogeneous calorimeter, with a length corresponding to approximately 25 nuclear interaction lengths, partially surrounding the active target to avoid any particle leakage from the calorimeter lateral faces.

4.4 Measurement and analysis strategy

The experiment will be characterised by a very high measurement rate, dominated by events with full en-

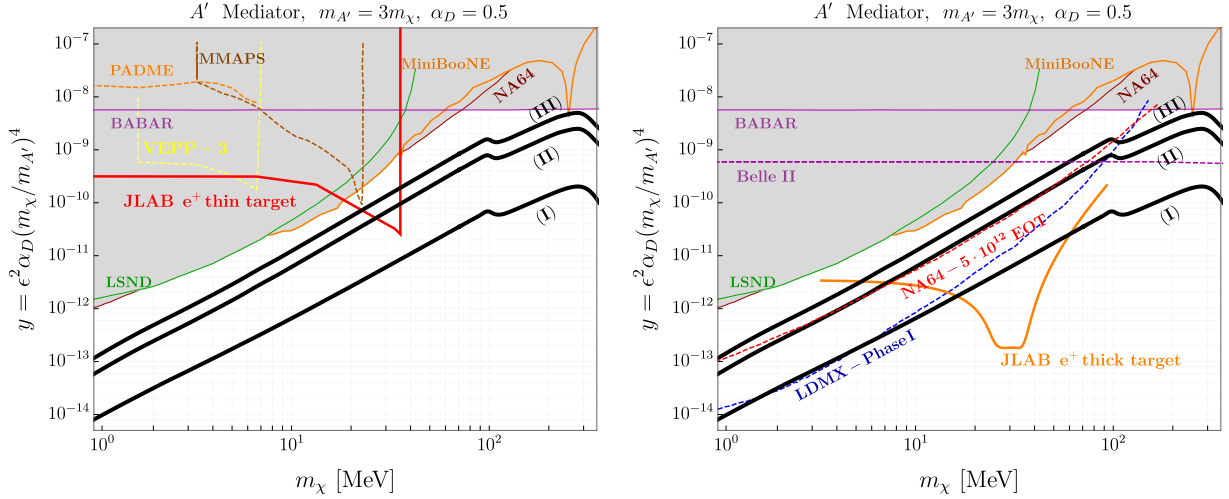


Fig. 8 The expected sensitivity for the thin-target (red, left) and thick-target (orange, right) measurements, compared to existing exclusion limits (grey area [51,52,53]) and projections for future efforts (dotted lines: PADME [54], MMAPS [55], VEPP-3 [56], Belle-II [57], LDMX [24] and NA64 [6]). The black lines are the thermal targets for pseudo-Dirac fermion LDM (I), Majorana fermion LDM (II) and elastic and inelastic scalar LDM (III).

ergy deposition in the calorimeter. To cope with this, the data acquisition system will be configured to record only events with a significant ($\gtrsim 1$ GeV) energy loss in the calorimeter. From a preliminary estimate, the expected trigger rate will be ~ 20 kHz, for a primary beam impinging with 2 MHz frequency on the detector. This minimum-bias condition will be initially studied with Montecarlo simulations, to evaluate the efficiency and confirm that no distortions to the experiment physics outcome are introduced. In parallel to the main production trigger, prescaled trigger conditions will be implemented to save full-energy events for calibration and monitoring. A blind approach to data analysis will be followed. First, events in the signal region, based on a preliminary choice of the calorimeter and hadron detection system energy cuts, will be excluded from the analysis. Then, the expected number of backgrounds will be evaluated using both Montecarlo simulations and events in the neighborhood of the signal region, in order to identify an optimal set of selection cuts for the signal that maximize the experiment sensitivity [58]. Finally, the signal region will be scrutinized.

5 Results

The 90% CL sensitivity of the two proposed measurements is shown in Fig. 8, compared with current exclusion limits (grey areas) and expected performance of other missing-energy / missing-mass future experiments (dashed curves). On the same plot, we show the thermal targets for significant variations of the minimal LDM model presented in the introduction: elastic and inelastic scalar LDM (I), Majorana fermion LDM

(II) and pseudo-Dirac fermion LDM (III). For the thin-target effort, the red curve reports the sensitivity estimate based on the realistic backgrounds that have been discussed before. For the thick-target case, the orange curve refers to the ideal case of a zero-background measurement, considering a 5.5 GeV missing energy threshold, and assuming an overall 50% signal efficiency. This hypothesis, following what was done in similar experiments [59,52], will be investigated with Montecarlo simulations during the future experiment design phase.

5.1 Complementarity of the two approaches

The two measurements that we presented in this document are characterized by different sensitivities and design complexity. They can be considered as two complementary experiments facing the light dark matter physical problem, and as such we foresee a comprehensive LDM physical program at JLab with both of them running, but with different time schedules.

With the availability of a 100-nA, 11-GeV positron beam at JLab, the thin-target experiment can start almost immediately, since no demanding requirements on the beam are present. The conceptual design is already mature, being based on realistic Monte Carlo simulations. Furthermore, the detector can be based on an already-existing and working setup, the PADME experiment at LNF [37]. As discussed before, the possibility of installing PADME at JLab, benefiting from both the existing equipment and our experience is a compelling possibility, allowing us to run successfully the thin-target measurements from day one.

Meanwhile, we propose starting the necessary R&D activity in preparation to the thick-target measurement, exploiting synergic activities at the laboratory in the context of the EIC program. The goal is to be ready to start the measurements on a time scale of few years after the beginning of the e^+ program at JLab.

6 Conclusions and outlook

In this document, we have discussed two complementary strategies to explore the phenomenology of dark sectors by exploiting a future e^+ beam at JLab. The unique properties of this facility – the high energy, the high intensity and the versatile operation mode – will allow these two experimental approaches to investigate vast unexplored regions in the parameters space, beyond those covered by current or planned experiments. An experimental program more comprehensive than the one discussed here can also be envisaged, which would include dedicated measurements to investigate more in depth some specific LDM scenarios. Possible efforts include, for example, dedicated measurements aimed to scrutinize the explanation in terms of a dark boson of the recently reported ^8Be and ^4He anomalies [15,16].

In summary, the availability of a positron beam will make JLab the premier facility for exploring the dark sector, and the proposed experimental program will allow for the confirmation or rejection of the LDM hypothesis by covering the thermal targets in a wide region in the parameters space.

This material is based upon work supported by the U.S. Department of Energy, Office of Science, Office of Nuclear Physics under contract DE-AC05-06OR23177.

References

1. G. Arcadi, M. Dutra, P. Ghosh, M. Lindner, Y. Mambrini, M. Pierre, S. Profumo, and F.S. Queiroz. The waning of the WIMP? A review of models, searches, and constraints. *Eur. Phys. J. C*, 78(3):203, 2018.
2. J.L. Feng et al. Planning the Future of U.S. Particle Physics (Snowmass 2013): Chapter 4: Cosmic Frontier. In *Community Summer Study 2013: Snowmass on the Mississippi*, 1 2014.
3. J.L. Hewett et al. Planning the Future of U.S. Particle Physics (Snowmass 2013): Chapter 2: Intensity Frontier. In *Community Summer Study 2013: Snowmass on the Mississippi*, 1 2014.
4. J. Alexander et al. Dark Sectors 2016 Workshop: Community Report. 8 2016.
5. M. Battaglieri et al. US Cosmic Visions: New Ideas in Dark Matter 2017: Community Report. In *U.S. Cosmic Visions: New Ideas in Dark Matter*, 7 2017.
6. J. Beacham et al. Physics Beyond Colliders at CERN: Beyond the Standard Model Working Group Report. *J. Phys. G*, 47(1):010501, 2020.
7. P. Agrawal et al. Feebly-Interacting Particles:FIPs 2020 Workshop Report. 2 2021.
8. T. Blum, A. Denig, I. Logashenko, E. de Rafael, B.L. Roberts, T. Teubner, and G. Venanzoni. The Muon ($g-2$) Theory Value: Present and Future. 11 2013.
9. R. Pohl et al. The size of the proton. *Nature*, 466:213–216, 2010.
10. C.E. Carlson. The Proton Radius Puzzle. *Prog. Part. Nucl. Phys.*, 82:59–77, 2015.
11. J.J. Krauth et al. The proton radius puzzle. In *52nd Rencontres de Moriond on EW Interactions and Unified Theories*, pages 95–102, 2017.
12. F.E. Wietfeldt and G.L. Greene. Colloquium: The neutron lifetime. *Rev. Mod. Phys.*, 83(4):1173–1192, 2011.
13. G.L. Greene and P. Geltenbort. The Neutron Enigma. *Scientific American*, 314:36–41, 2016.
14. L. Sbordone, P. Bonifacio, E. Caffau, H. G. Ludwig, N. T. Behara, J. I. González Hernández, M. Steffen, R. Cayrel, B. Freytag, C. Van’t Veer, and et al. The metal-poor end of the spite plateau. *Astronomy & Astrophysics*, 522:A26, Oct 2010.
15. A.J. Krasznahorkay et al. Observation of anomalous internal pair creation in ^8Be : A possible indication of a light, neutral boson. *Phys. Rev. Lett.*, 116:042501, Jan 2016.
16. A.J. Krasznahorkay et al. New evidence supporting the existence of the hypothetical X17 particle. 10 2019.
17. E. Nardi, C.D.R. Carvajal, A. Ghoshal, D. Meloni, and M. Raggi. Resonant production of dark photons in positron beam dump experiments. *Phys. Rev. D*, 97(9):095004, 2018.
18. L. Marsicano, M. Battaglieri, M. Bondi, C. D.R. Carvajal, A. Celentano, M. De Napoli, R. De Vita, E. Nardi, M. Raggi, and P. Valente. Dark photon production through positron annihilation in beam-dump experiments. *Phys. Rev. D*, 98(1):015031, 2018.
19. L. Marsicano, M. Battaglieri, M. Bondi, C.D.R. Carvajal, A. Celentano, M. De Napoli, R. De Vita, E. Nardi, M. Raggi, and P. Valente. Novel Way to Search for Light Dark Matter in Lepton Beam-Dump Experiments. *Phys. Rev. Lett.*, 121(4):041802, 2018.
20. A. Celentano, L. Darmé, L. Marsicano, and E. Nardi. New production channels for light dark matter in hadronic showers. *Phys. Rev. D*, 102(7):075026, 2020.
21. T.R. Slatyer, N. Padmanabhan, and D.P. Finkbeiner. CMB Constraints on WIMP Annihilation: Energy Absorption During the Recombination Epoch. *Phys. Rev. D*, 80:043526, 2009.
22. T.R. Slatyer. Indirect dark matter signatures in the cosmic dark ages. I. Generalizing the bound on s-wave dark matter annihilation from Planck results. *Phys. Rev. D*, 93(2):023527, 2016.
23. N. Aghanim et al. Planck 2018 results. VI. Cosmological parameters. 2018.
24. A. Berlin, N. Blinov, G. Krnjaic, P. Schuster, and N. Toro. Dark Matter, Millicharges, Axion and Scalar Particles, Gauge Bosons, and Other New Physics with LDMX. *Phys. Rev. D*, 99(7):075001, 2019.
25. David Tucker-Smith and Neal Weiner. Inelastic dark matter. *Phys. Rev. D*, 64:043502, 2001.
26. E. Izaguirre, G. Krnjaic, and B. Shuve. Discovering Inelastic Thermal-Relic Dark Matter at Colliders. *Phys. Rev. D*, 93(6):063523, 2016.

27. K. Griest and D. Seckel. Three exceptions in the calculation of relic abundances. *Phys. Rev. D*, 43:3191–3203, 1991.
28. E. Izaguirre, Y. Kahn, G. Krnjaic, and M. Moschella. Testing Light Dark Matter Coannihilation With Fixed-Target Experiments. *Phys. Rev.*, D96(5):055007, 2017.
29. J.L. Feng and J. Smolinsky. Impact of a resonance on thermal targets for invisible dark photon searches. *Phys. Rev. D*, 96(9):095022, 2017.
30. S.-M. Choi, Y.-J. Kang, and H.M. Lee. On thermal production of self-interacting dark matter. *JHEP*, 12:099, 2016.
31. L. Darmé, S. Rao, and L. Roszkowski. Light dark Higgs boson in minimal sub-GeV dark matter scenarios. *JHEP*, 03:084, 2018.
32. L. Darmé, S. Rao, and L. Roszkowski. Signatures of dark Higgs boson in light fermionic dark matter scenarios. *JHEP*, 12:014, 2018.
33. A. Celentano. The Heavy Photon Search experiment at Jefferson Laboratory. *J. Phys. Conf. Ser.*, 556(1):012064, 2014.
34. G.B. Franklin. The APEX experiment at JLab. Searching for the vector boson A' decaying to e^+e^- . *EPJ Web Conf.*, 142:01015, 2017.
35. L. Marsicano. The Beam Dump eXperiment. *PoS*, ICHEP2018:075, 2019.
36. R. Corliss. Searching for a dark photon with DarkLight. *Nucl. Instrum. Meth. A*, 865:125–127, 2017.
37. M. Raggi and V. Kozhuharov. Proposal to Search for a Dark Photon in Positron on Target Collisions at DAΦNE Linac. *Adv. High Energy Phys.*, 2014:959802, 2014.
38. E. Izaguirre et al. Testing GeV-scale dark matter with fixed-target missing momentum experiments. *Phys. Rev. D*, 91:094026, May 2015.
39. A. Pukhov. Calcchep 2.3: Mssm, structure functions, event generation, batchs, and generation of matrix elements for other packages, 2004.
40. S. Agostinelli et al. GEANT4: A Simulation toolkit. *Nucl. Instrum. Meth.*, A506:250–303, 2003.
41. E. Leonardi, V. Kozhuharov, M. Raggi, and P. Valente. GEANT4-based full simulation of the PADME experiment at the DAΦNE BTF. *J. Phys. Conf. Ser.*, 898(4):042025, 2017.
42. M. Raggi et al. Performance of the PADME Calorimeter prototype at the DAΦNE BTF. *Nucl. Instrum. Meth. A*, 862:31–35, 2017.
43. E. Leonardi, M. Raggi, and P. Valente. Development and test of a DRS4-based DAQ system for the PADME experiment at the DAΦNE BTF. *J. Phys. Conf. Ser.*, 898(3):032024, 2017.
44. M. Tanabashi et al. Review of particle physics. *Phys. Rev. D*, 98:030001, Aug 2018.
45. A.B. Chilton. A note on the fluence concept. *Health Physics*, 34(6):715–716, 1978.
46. J. Grames and E. Voitier. Private communication, 2020.
47. P. Adzic et al. Radiation hardness qualification of PbWO(4) scintillation crystals for the CMS Electromagnetic Calorimeter. *JINST*, 5:P03010, 2010.
48. S. Chatrchyan et al. The CMS Experiment at the CERN LHC. *JINST*, 3:S08004, 2008.
49. V. Dormenev et al. Stimulated recovery of the optical transmission of pbwo4 scintillation crystals for electromagnetic calorimeters after radiation damage. *Nucl. Instrum. Meth. A*, 623(3):1082 – 1085, 2010.
50. S. Fegan et al. Assessing the performance under ionising radiation of lead tungstate scintillators for EM calorimetry in the CLAS12 Forward Tagger. *Nucl. Instrum. Meth.*, A789:101–108, 2015.
51. J.P. Lees et al. Search for Invisible Decays of a Dark Photon Produced in e^+e^- Collisions at BaBar. *Phys. Rev. Lett.*, 119(13):131804, 2017.
52. D. Banerjee et al. Dark matter search in missing energy events with NA64. *Phys. Rev. Lett.*, 123(12):121801, 2019.
53. A.A. Aguilar-Arevalo et al. Dark Matter Search in Nucleon, Pion, and Electron Channels from a Proton Beam Dump with MiniBooNE. *Phys. Rev.*, D98(11):112004, 2018.
54. M. Raggi, V. Kozhuharov, and P. Valente. The PADME experiment at LNF. *EPJ Web Conf.*, 96:01025, 2015.
55. Alexander, J. Mmaps: Missing-mass a-prime search. *EPJ Web Conf.*, 142:01001, 2017.
56. B. Wojtsekhowski et al. Searching for a dark photon: Project of the experiment at VEPP-3. *JINST*, 13(02):P02021, 2018.
57. W. Altmannshofer et al. The Belle II Physics Book. *PTEP*, 2019(12):123C01, 2019. [Erratum: PTEP 2020, 029201 (2020)].
58. G. Cowan et al. Asymptotic formulae for likelihood-based tests of new physics. *Eur. Phys. J.*, C71:1554, 2011. [Erratum: Eur. Phys. J.C73,2501(2013)].
59. T. Åkesson et al. Light Dark Matter eXperiment (LDMX), 2018.